Trapped-Ion Quantum Simulation of an Ising Model with Transverse and Longitudinal Fields

P. Richerme[1], C. Senko[1], S. Korenblit[1], J. Smith[1], A. Lee,[1] W. C. Campbell,[2] and C. Monroe[1]

[1] *Joint Quantum Institute, University of Maryland Department of Physics and National Institute of Standards and Technology, College Park, MD 20742*

[2] *Department of Physics and Astronomy, University of California, Los Angeles, CA 90095*

(Dated: March 29, 2013)

We perform a quantum simulation of an Ising model with long-range interactions and both transverse and longitudinal fields – the most general external field configuration – in a system of 6 to 10 trapped atomic ions. Quantum fluctuations at zero temperature drive the ground state spin ordering through several classical first-order phase transitions as the strength of the longitudinal field is increased. The Hamiltonian under study generates a fractal Devil's staircase structure and maps onto a large number of many-body and energy-optimization problems, showing how quantum simulation can potentially find solutions that are classically intractable.

Many-body quantum systems, such as high-T_C superconductors [1] or complex configurations of interacting spins [2–5], are often difficult to describe analytically or calculate numerically on account of the exponential scaling of the Hilbert space with the system size. For instance, predicting the behavior of some simple quantum spin models is currently limited to just a few dozen spins [6], while solving a fully-connected frustrated Ising model is known to be an NP-complete problem [7]. Instead, quantum simulators, in which a well-controlled quantum system is used to simulate a system of interest [8, 9], may be employed to calculate ground state or dynamical properties of a Hamiltonian that would otherwise prove classically intractable or non-integrable.

Quantum simulators require excellent coherence properties and high-fidelity readout and control. To date, simple quantum simulations have been performed in a variety of systems, using neutral atoms in optical lattices [10–12], nuclear magnetic resonance [13], photons [14, 15], and trapped atomic ions [16–25]. Early trapped ion simulations of many-body physics demonstrated tunable spin-spin interactions [16, 17], engineered entangled spin states through dissipation [20], and observed the onset of a quantum phase transition as the number of spins was increased from 2 to 9 [21]. Initial studies of frustration within the context of the antiferromagnetic (AFM) Ising model [18] were later enhanced by tuning the range of interaction and the degree of frustration in a system of up to 16 spins [24].

In this Letter, we report the first quantum simulation of an AFM Ising model with long-range interactions and both transverse and longitudinal magnetic fields. The addition of the longitudinal field allows for the application of an arbitrary magnetic field relative to the Ising couplings and the creation and observation of new spin phases at zero temperaure. As the strength of the longitudinal field is increased from $B_x = 0$, the system passes through $N/2$ first-order phase transitions driven by quantum fluctuations, where N is the number of spins. Determination of the ground state spin ordering for differing longitudinal fields reveals a Wigner-crystal spin structure [26], maps on to a number of energy minimization problems [27, 28], and shows hints of a complete Devil's staircase [29] which would emerge for convex long-range interactions as $N \to \infty$.

The system is described by the Hamiltonian

$$H = \sum_{i<j} J_{i,j}\sigma_x^{(i)}\sigma_x^{(j)} + B_x \sum_i \sigma_x^{(i)} + B_y(t) \sum_i \sigma_y^{(i)} \quad (1)$$

where $J_{i,j}$ gives the strength of the Ising coupling between spins i and j, B_x is the magnitude of the longitudinal magnetic field, $B_y(t)$ is a time-dependent transverse field, and $\sigma_\alpha^{(i)}$ is the Pauli spin operator for the ith particle along the α direction. We tune $J_{i,j} > 0$ to generate AFM interactions between the spins that fall off with distance. At $t = 0$ the spins are initialized to point along the direction of the total magnetic field $\vec{B} = B_x\hat{x} + B_y(0)\hat{y}$, with $B_y(0) \gg J$, which is the instantaneous ground state of the Hamiltonian in Eqn. 1 to good approximation. The system will remain in the ground state if the transverse field $B_y(t)$ is ramped down adiabatically. The resulting spin order at the end of the ramp when $B_y = 0$ would then reveal the ground state of an Ising Hamiltonian with long-range interactions and a longitudinal field.

Fig. 1(a) shows the energy eigenvalues obtained by diagonalizing Eqn. 1 when $B_y = 0$ for a system with 6 spins. The ground state passes through three level crossings as the strength of the longitudinal field B_x is increased from $B_x = 0$, indicating three first-order phase transitions separating four distinct spin phases. When B_x is set at a phase transition and $B_y(t)$ is ramped down, as in Fig. 1(b), the critical gap between the ground and first coupled excited state closes on account of the degeneracy of spin orderings at the phase transition.

Long-range interactions allow for the creation of many more spin phases compared with a nearest-neighbor-only Ising model. Consider a nearest-neighbor AFM model

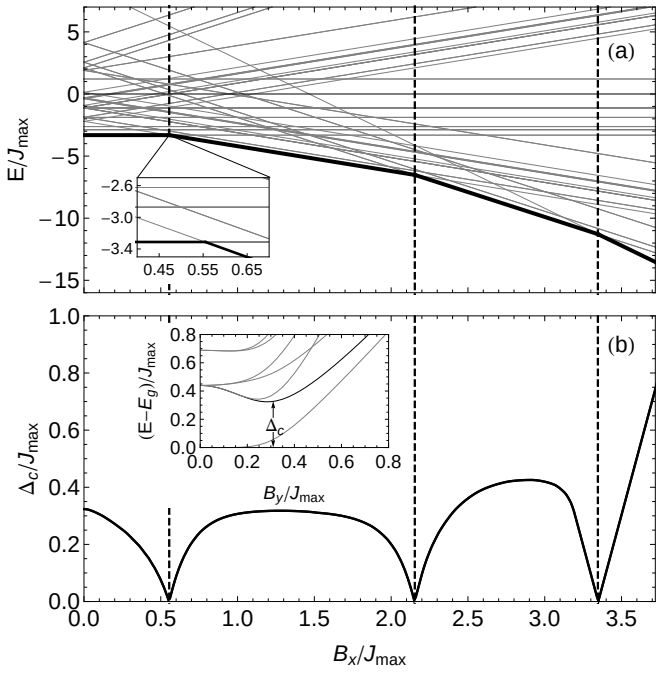

FIG. 1. (a) Low-lying energy eigenvalues of Eqn. 1 for $B_y = 0$ and $N = 6$, with the long-range $J_{i,j}$ couplings determined from experimental conditions (see text). Level crossings (inset) indicate the presence of first-order phase transitions in the ground state. (b) The critical gap Δ_c between the ground state energy E_g and first coupled excited state energy shrinks to zero at the three phase transitions (vertical dashed lines). Inset: low-lying energy levels of Eqn. 1 as the transverse field B_y is varied with $B_x = 0$.

with $N/2$ "up" spins, N total spins, and a ground-state ordering $|..\downarrow\uparrow\downarrow\uparrow\downarrow\uparrow..\rangle_x$. An excited state at $B_x = 0$ may have an additional spin polarized along $|\downarrow\rangle_x$, either by making a kink of type $|..\downarrow\uparrow\downarrow\downarrow\uparrow\downarrow..\rangle_x$ or a spin defect of type $|..\downarrow\uparrow\downarrow\downarrow\downarrow\uparrow..\rangle_x$. The interaction energy cost of making n kinks is $2nJ$, while the field energy gain is $2nB_x$. At $B_x/J = 1$ multiple energy levels intersect to give a first-order phase transition. Similarly, the energy cost of making n spin defects is $4nJ$ and the gain is $2nB_x$, so a second phase transition occurs at $B_x/J = 2$. Only three different spin phases are observable as B_x is varied from $0 \to \infty$, independent of N, and there is a large degeneracy of spin eigenstates at the phase transitions. The presence of long-range interactions lifts this degeneracy and admits $N/2+1$ distinct spin phases, with $\{0, 1, \ldots, N/2\}$ spins in state $|\uparrow\rangle_x$.

Observation of these $N/2+1$ classical phases is made possible only by quantum fluctuations in our quantum simulator. The second term in Eq. 1 commutes with the first, so the system is classical when $B_y = 0$. However, varying B_x across a phase boundary in a zero temperature system does not lead to a new ground state, since thermal fluctuations are required to drive the transition. Observation of spin phases at intermediate values of B_x and zero temperature thus requires quantum fluctuations [30], which are provided by the non-commuting third term in the Hamiltonian (Eqn. 1).

The effective spin system is encoded in a linear chain of trapped ^{171}Yb ions [31], with zero effective spin temperature. The spin states $|\uparrow\rangle_z$ and $|\downarrow\rangle_z$ are represented by the hyperfine clock states $^2S_{1/2}\ |F = 1, m_F = 0\rangle$ and $|F = 0, m_F = 0\rangle$, respectively, which have a frequency splitting of $\omega_S/2\pi = 12.642819$ GHz [32]. A weak magnetic field of ~ 5 G defines the quantization axis. The states are detected by illuminating the ions with laser light resonant with the $^2S_{1/2}$ to $^2P_{1/2}$ cycling transition at 369.5 nm and imaging the spin-dependent fluorescence. Either $N = 6$ or $N = 10$ ions are confined in a three-layer rf Paul trap with a center-of-mass axial trap frequency $f_z = 0.7$ MHz and transverse frequencies $f_x = 4.8$ MHz and $f_y = 4.6$ MHz and interact with each other via their collective modes of motion.

The Ising couplings $J_{i,j}$ are generated by globally irradiating the ions with two off-resonant $\lambda = 355$ nm laser beams which drive stimulated Raman transitions [33, 34]. The beams intersect at right angles so that their wavevector difference $\Delta\vec{k}$ points along the x-direction of transverse ion motion, perpendicular to the linear chain. Acousto-optic modulators imprint beatnote frequencies of $\omega_S \pm \mu$ between the beams, imparting a spin-dependent optical dipole force at frequency μ [35]. In the limit where the beatnotes are sufficiently far from the transverse normal modes ω_m, we obtain a spin-spin coupling given by

$$J_{i,j} = \Omega_i \Omega_j \frac{\hbar(\Delta\vec{k})^2}{2M} \sum_m \frac{b_{i,m} b_{j,m}}{\mu^2 - \omega_m^2} \qquad (2)$$

in the Lamb-Dicke limit, where Ω_i is the Rabi frequency of the ith ion, M is the single ion mass, and $b_{i,m}$ is the normal-mode transformation matrix for ion i in mode m [17]. The Ising interactions are long-range and fall off approximately as $J_{i,j} \sim 1/|i-j|^\alpha$, with $\alpha = 0.94$ for $N = 6$ and $\alpha = 0.83$ for $N = 10$.

The effective transverse and longitudinal magnetic fields $B_y(t)$ and B_x drive Rabi oscillations between the spin states $|\downarrow\rangle_z$ and $|\uparrow\rangle_z$. Each effective field is generated by a pair of Raman laser beams with a beatnote frequency of ω_S, with the field amplitude determined by the beam intensities. The field directions are controlled through the beam phases relative to the average phase φ of the two sidebands which give rise to the $\sigma_x\sigma_x$ interaction in Eqn. 2. In particular, an effective field phase offset of 0° (90°) relative to φ generates a σ_y (σ_x) interaction.

Each experiment begins with 3 ms of Doppler cooling, followed by optical pumping to the state $|\downarrow\downarrow\downarrow..\rangle_z$ and 100 μs of Raman sideband cooling that prepares the motion of all modes along $\Delta\vec{k}$ in the Lamb-Dicke limit. The spins are then coherently rotated into the equatorial plane of the Bloch sphere so that they point along the

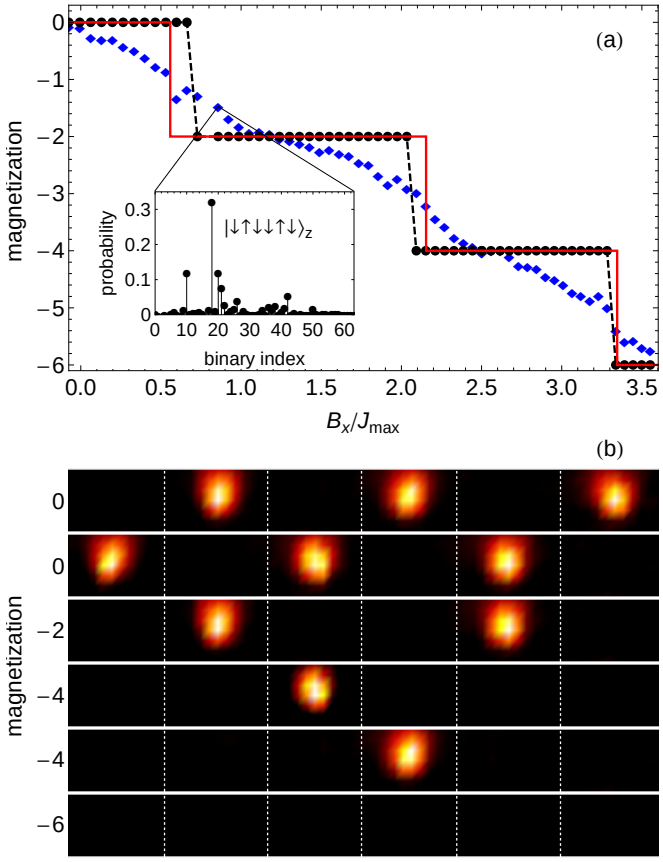

FIG. 2. (Color) (a) Magnetization ($m_z = N_\uparrow - N_\downarrow$) of a chain of 6 ions for increasing axial field strength. Red, solid: predicted magnetization value, with the step locations indicating the first-order phase transitions. Blue diamonds: average magnetization of 4000 experiments performed at each value of B_x. Black, dashed: magnetization of the most probable state (see inset) found at each B_x value. (b) Camera images of the ground states found at each step in (a): $|\downarrow\uparrow\downarrow\uparrow\downarrow\uparrow\rangle_z$ and $|\uparrow\downarrow\uparrow\downarrow\uparrow\downarrow\rangle_z$ ($m_z = 0$), $|\downarrow\uparrow\downarrow\downarrow\uparrow\downarrow\rangle_z$ ($m_z = -2$), $|\downarrow\downarrow\uparrow\downarrow\downarrow\downarrow\rangle_z$ and $|\downarrow\downarrow\downarrow\uparrow\downarrow\downarrow\rangle_z$ ($m_z = -4$), and $|\downarrow\downarrow\downarrow\downarrow\downarrow\downarrow\rangle_z$ ($m_z = -6$).

direction $\vec{B} = B_x\hat{x} + B_y(0)\hat{y}$, where B_x is varied between different simulations. The Hamiltonian (Eqn. 1) is then switched on at $t = 0$ with the chosen value of B_x and $B_y(0) = 5J_{max}$, where J_{max} is the largest spin-spin coupling (typically $2\pi\times$0.6-0.7 kHz). The transverse field is ramped down to $B_y \approx 0$ exponentially with a time constant of 600 μs and a total time of 3 ms, with the ramp times chosen to minimize decoherence effects while maximizing adiabaticity. At $t = 3$ ms, the Hamiltonian is switched off and the $x-$component of each spin is measured by applying a global $\pi/2$ rotation about the $\hat{y}$ axis, illuminating the ions with resonant light, and imaging the spin-dependent fluorescence using an intensified CCD camera (Princeton Instruments PIMax3:1024i). The experiments are repeated 4000 times to determine the probability of each possible spin configuration.

The camera measurement cycle for each experiment takes 10 ms, with 3 ms of fluorescence collection, 3 ms of phosphor decay from the CCD intensifier, and 3.6 ms of readout time. For all data, we restrict the region of interest on the CCD to an approximately 128×7 bin window to speed readout from the device. We compensate for detection errors ($\epsilon = 7\%$ for a single spin) by multiplying a matrix describing the expected multi-spin error by the vector containing the measured probability of each spin configuration [36].

We investigate the order parameter of net magnetization, $m_z = N_\uparrow - N_\downarrow$ as we vary the strength of the longitudinal field B_x. The magnetization of the ground state spin ordering of Eq. 1 is expected to yield a staircase with sharp steps at the phase transitions (red line in Fig. 2(a)) when $B_y = 0$ [29]. The experimental data (blue points in Fig. 2(a)) show an averaged magnetization with heavily broadened steps due largely to non-adiabatic evolution during the exponential ramp that populate excited states. However, the ground state spin configuration at each value of B_x may be extracted by looking at the probability distribution of all spin states and selecting the most prevalent state (inset of Fig. 2(a)) [37]. The magnetization of the spin states found by this method (black points in Fig. 2(a)) agree well with the theoretical prediction.

Direct images of the ground state spin phases are shown in Fig. 2(b), with approximately 1000 averaged images per line. Each box contains an ion that scatters many photons when in the state $|\uparrow\rangle_z$ and essentially no photons when in the state $|\downarrow\rangle_z$. For magnetizations of 0 and -4, two ground state orderings are observed due to the left-right symmetry of the spin-spin interactions. In cases where left-right reflection of the spin chain produces a new spin ordering with degenerate energy, the summed probability of both states is used when determining the most probable state.

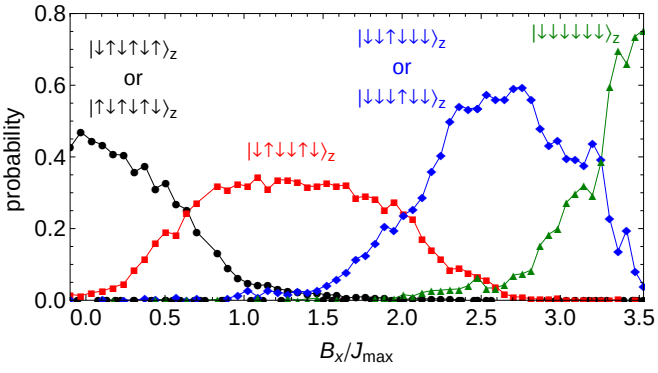

FIG. 3. (Color Online) Probabilities of the 4 different ground state spin phases as B_x is varied in a 6-ion system. Black dots: $|\downarrow\uparrow\downarrow\uparrow\downarrow\uparrow\rangle_z$ or $|\uparrow\downarrow\uparrow\downarrow\uparrow\downarrow\rangle_z$. Red squares: $|\downarrow\uparrow\downarrow\downarrow\uparrow\downarrow\rangle_z$. Blue diamonds: $|\downarrow\downarrow\uparrow\downarrow\downarrow\downarrow\rangle_z$ or $|\downarrow\downarrow\downarrow\uparrow\downarrow\downarrow\rangle_z$. Green triangles: $|\downarrow\downarrow\downarrow\downarrow\downarrow\downarrow\rangle_z$

The probability of populating the four distinct ground states as B_x is varied, shown in Fig. 3, further probes

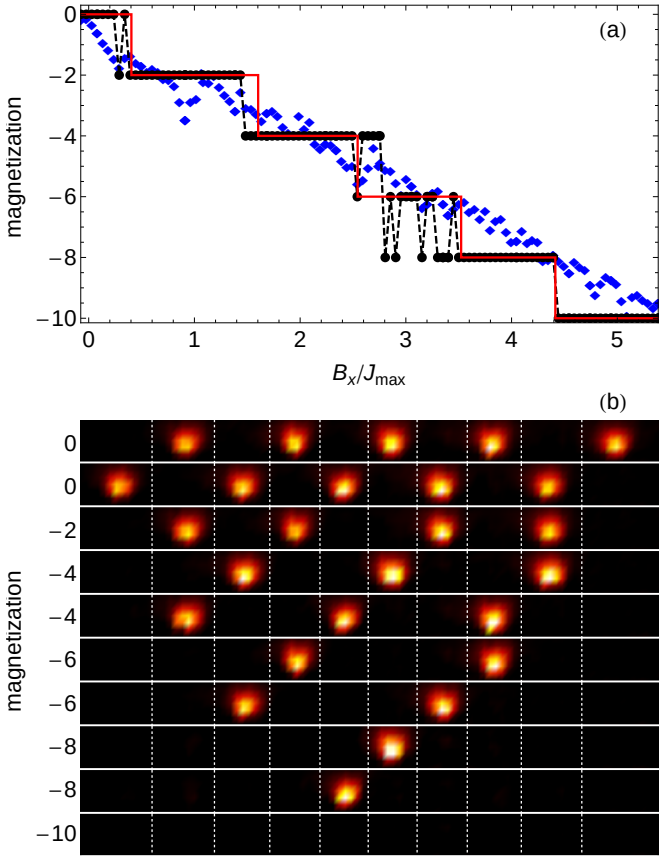

FIG. 4. (Color) (a) Magnetization of a chain of 10 ions for increasing axial field strength. The red, blue, and black curves correspond to the theoretical magnetization, average measured magnetization, and magnetization of the most probable state (respectively) for increasing B_x. (b) Camera images of the theoretical ground states found experimentally at each step in (a).

the multiple phase transitions. Fig. 1 shows that as $B_x/J_{\max}$ approaches a phase transition, the energy levels of the spin eigenstates on opposing sides of the transition cross, and the critical gap Δ_c between them shrinks. The smooth crossover between the four distinct ground-state spin phases in Fig. 3 therefore arises from increasingly diabatic simulations near the energy-level crossings at the first-order transitions. Comparing with Fig. 1(b), we find higher probabilities of creating the theoretical ground state when the critical gap Δ_c is large. Simulations that are more adiabatic could be expected to give both larger maximum probabilities in each of the four different ground states and sharper crossovers between the state populations near the phase transitions.

Figure 4 plots the magnetization of a 10-ion chain for increasing strengths of the longitudinal field B_x, along with the associated camera images of the $N/2+1=6$ distinct ground state phases. Similarly to the 6-ion case, we experimentally determine the ground state ordering by selecting the most prevalent of the $2^{10}=1024$ possible states. Because the critical gap Δ_c is much smaller for a 10-ion system, the reduction of the transverse field $B_y(t)$ is much less adiabatic, and only $\sim 5\%$ of the total population lands in the theoretical ground state for much of the data in Fig. 4(a). We are therefore more sensitive to experimental error sources (of order a few percent) such as imperfect initialization and slow drifts in the strength of $J_{i,j}$, as well as statistically-limited quantum projection noise of order $\approx 1\%$.

For the 10-ion chain, Fig. 4(b) shows the interesting spin structure that emerges as B_x is varied. For a given B_x and associated number of bright ions q, the ground-state spin configuration of Eqn. 1 (with $B_y=0$) solves the problem of finding the lowest energy arrangement of q charged particles on N lattice sites. The creation of such periodic spin structures realizes a generalized Wigner crystal, which is the configuration adopted by a low-density electron gas when the Coulomb repulsion dominates over the kinetic energy [38]. As the system size $N\to\infty$ and B_x is increased, the magnetization reveals a fractal staircase structure that arises since every rational filling factor (of which there are infinitely many) is the ground state for some value of B_x [29].

In conclusion, we have performed a quantum simulation of an Ising model with both transverse and longitudinal magnetic fields within a linear chain of trapped ions. Long-range spin-spin couplings enabled the existence of a large number of ground state spin phases at zero temperature, while quantum fluctuations inherent in our quantum simulations enabled their observation. As the system size is scaled up, such quantum simulations can begin to solve diverse problems in many-body physics where classical calculation becomes intractable.

This work is supported by the U.S. Army Research Office (ARO) Award W911NF0710576 with funds from the DARPA Optical Lattice Emulator Program, ARO award W911NF0410234 with funds from the IARPA MQCO Program, and the NSF Physics Frontier Center at JQI.

[1] S. Sachdev, Rev. Mod. Phys. **75**, 913 (2003).
[2] K. Binder and A. P. Young, Rev. Mod. Phys. **58**, 801 (1986).
[3] L. Balents, Nature **464**, 199 (2010).
[4] S. T. Bramwell and M. J. P. Gingras, Science **294**, 1495 (2001).
[5] C. M. Dawson and M. A. Nielsen, Phys. Rev. A **69**, 052316 (2004).
[6] A. W. Sandvik, Phys. Rev. Lett. **104**, 137204 (2010).
[7] F. Barahona, J. Phys. A: Math. Gen. **15**, 3241 (1982).
[8] R. Feynman, Int. J. Theor. Phys. **21**, 467 (1982).
[9] S. Lloyd, Science **273**, 1073 (1996).
[10] C. Weitenberg *et al.*, Nature **471**, 319 (2011).
[11] D. Greif *et al.*, Phys. Rev. Lett. **106**, 145302 (2011).
[12] J. Simon *et al.*, Nature **472**, 307 (2011).
[13] X. Peng, J. Zhang, J. Du, and D. Suter, Phys. Rev. Lett.

103, 140501 (2009).
[14] A. Aspuru-Guzik and P. Walther, Nat. Phys. **8**, 285 (2012).
[15] M. A. Broome *et al.*, Science **339**, 794 (2013).
[16] A. Friedenauer *et al.*, Nature Physics **4**, 757 (2008).
[17] K. Kim *et al.*, Phys. Rev. Lett. **103**, 120502 (2009).
[18] K. Kim *et al.*, Nature **465**, 590 (2010).
[19] E. E. Edwards *et al.*, Phys. Rev. B **82**, 060412 (2010).
[20] J. T. Barreiro *et al.*, Nature **470**, 486 (2011).
[21] R. Islam *et al.*, Nature Communications **2**, 377 (2011).
[22] B. P. Lanyon *et al.*, Science **334**, 57 (2011).
[23] J. W. Britton *et al.*, Nature **484**, 489 (2012).
[24] R. Islam *et al.*, Science (in press) (2013).
[25] A. Khromova *et al.*, Phys. Rev. Lett. **108**, 220502 (2012).
[26] E. Wigner, Phys. Rev. **46**, 1002 (1934).
[27] K. Katayama and H. Narihisa, Eur. J. of Oper. Res. **134**, 103 (2001).
[28] A. Perdomo-Ortiz *et al.*, Nature Sci. Reports **2**, 571 (2012).
[29] P. Bak and R. Bruinsma, Phys. Rev. Lett. **49**, 249 (1982).
[30] S. Sachdev, *Quantum Phase Transitions* (Cambridge Univ. Press, Cambridge, 1999).
[31] D. Porras and J. I. Cirac, Phys. Rev. Lett. **92**, 207901 (2004).
[32] S. Olmschenk *et al.*, Phys. Rev. A **76**, 052314 (2007).
[33] D. Hayes *et al.*, Phys. Rev. Lett. **104**, 140501 (2010).
[34] W. C. Campbell *et al.*, Phys. Rev. Lett. **105**, 090502 (2010).
[35] A. Sørensen and K. Mølmer, Phys. Rev. A **62**, 022311 (2000).
[36] C. Shen and L.-M. Duan, New J. Phys. **14**, 053053 (2012).
[37] P. Richerme *et al.*, in preparation (2013).
[38] J. Hubbard, Phys. Rev. B **17**, 494 (1978).